Time-Resolved Spectroscopy of the Early Photolysis Intermediates of Rhodopsin Schiff Base Counterion Mutants†

Stefan Jäger,‡ James W. Lewis,‡ Tatyana A. Zvyaga,§ Istvan Szundi,‡ Thomas P. Sakmar,§ and David S. Kliger*,‡

Department of Chemistry and Biochemistry, University of California, Santa Cruz, California 95064, and The Howard Hughes Medical Institute, Laboratory of Molecular Biology and Biochemistry, Rockefeller University, 1230 York Avenue, New York, New York 10021

Received September 16, 1996; Revised Manuscript Received December 11, 1996⊗

ABSTRACT: Time-resolved absorption difference spectra of COS-cell expressed rhodopsin and rhodopsin mutants (E113D, E113A/A117E, and G90D), solubilized in detergent, were collected from 20 ns to 510 ms after laser photolysis with 7 ns pulses (λ_{max} = 477 nm). The data were analyzed using a global exponential fitting procedure following singular value decomposition (SVD). Over the entire time range excellent agreement was achieved between results for COS-cell and rod outer segment rhodopsin both in kinetics and in the λ_{max} values of the intermediates. The Schiff base counterion mutant E113D showed strong similarities to rhodopsin up to lumi, following the established scheme: batho ⇌ bsi → lumi. Including late delay times (past 1 μs), the mutant E113D lumi decayed to metarhodopsin II (MII), showing that the detergent strongly favors MII over metarhodopsin I (MI). However, a back-reaction from MII to lumi was observed that was not seen for rhodopsin. The kinetic schemes for the mutants E113A/A117E and G90D were significantly different from that of rhodopsin. In both mutants batho decay into an equilibrium with bsi was too fast to resolve (<20 ns). The batho/bsi mixtures decayed with the following reaction scheme: batho/bsi ⇌ lumi ⇌ MI-like ⇌ MII-like. However, the back-reaction from MI-like to lumi was not seen in G90D. MI-like spectral intermediates absorbing around 460 nm appeared in both mutants. They have been shown to be the transducin-activating species (R*). These data, interpreted in the context of previous NMR, FTIR, and Raman data, are consistent with a picture in which the kinetics of batho decay is dependent on a protein-induced perturbation near $C_{12}-C_{13}$ of the retinal chromophore. The λ_{max} values of the bsi and lumi intermediates in the mutant pigments are interpreted in terms of movement of the Schiff base relative to its counterion.

Considerable progress has been made in understanding structure−function relationships in rhodopsin, as well as in its photointermediates, through UV−visible, resonance Raman, Fourier-transform infrared (FTIR),[1] NMR, and transducin activation experiments on native and mutant pigments (Fahmy et al., 1995; Palings et al., 1987; Han & Smith, 1995; Siebert, 1995; Kliger & Lewis, 1995; Sakmar & Fahmy, 1995; Hofmann et al., 1995). In the native pigment, 11-*cis*-retinal is bound via a protonated Schiff base to Lys^{296} located in transmembrane (TM) helix 7. The counterion to the protonated Schiff base has been identified as Glu^{113} (Sakmar et al., 1989; Zhukovsky & Oprian, 1989; Nathans, 1990) located in TM helix 3 (Figure 1). Light-induced cis−trans isomerization of the chromophore leads to the first intermediate, batho, within ≈10 ps (Yan et al., 1991; Popp et al., 1995). In this batho intermediate, the chromophore has been shown to be twisted, as demonstrated by hydrogen-out-of-plane (HOOP) modes of the retinal detected by resonance Raman and FTIR spectroscopies (Eyring et al., 1980, 1982; Fahmy et al., 1989, 1991; Palings et al., 1987). The Schiff base (SB) environment, on the other hand, seems not to be altered (C=N stretching vibration- and deuterium-induced downshifts are the same in batho and in the parent pigment). This evidence, along with results of NMR studies, shows that it is likely that the red shift in batho is primarily due to twisting of the chromophore, as well as to the altered orientation of the negative charge of the counterion relative to the retinal plane (Han & Smith, 1995).

Nanosecond time-resolved spectroscopy of native and artificial rhodopsin (rho) has proven very useful in recent years for identifying early photolysis intermediates [bathorhodopsin (batho), blue-shifted intermediate (bsi), and lumirhodopsin (lumi)] of visual pigments (Lewis et al., 1989; Hug et al., 1990; Kliger & Lewis, 1995). These studies have shown that the use of time-resolved measurements of photolysis intermediates at near physiological temperatures allows for the identification and characterization of intermediates which are not detectable in low-temperature trapping experiments. Thus, while the mechanism for the early photolysis intermediates deduced from low-temperature trapping experiments is

† This work was supported in part by NIH Grant EY00983 to D.S.K. T.P.S. is an Associate Investigator and T.A.Z. is an Associate of the Howard Hughes Medical Institute.

* To whom correspondence may be addressed.
‡ University of California.
§ Rockefeller University.

⊗ Abstract published in *Advance ACS Abstracts,* February 1, 1997.

[1] Abbreviations: FTIR, Fourier-transform infrared; HOOP, hydrogen out of plane; NMR, nuclear magnetic resonance; rho, rhodopsin; R*, light-activated pigment; batho, bathorhodopsin; bsi, blue-shifted intermediate of rho; lumi, lumirhodopsin; meta I or MI, metarhodopsin I; meta II or MII, metarhodopsin II; ROS, rod outer segment; SB, Schiff base; SVD, singular value decomposition; TM, transmembrane.

S0006-2960(96)02320-3 CCC: $14.00

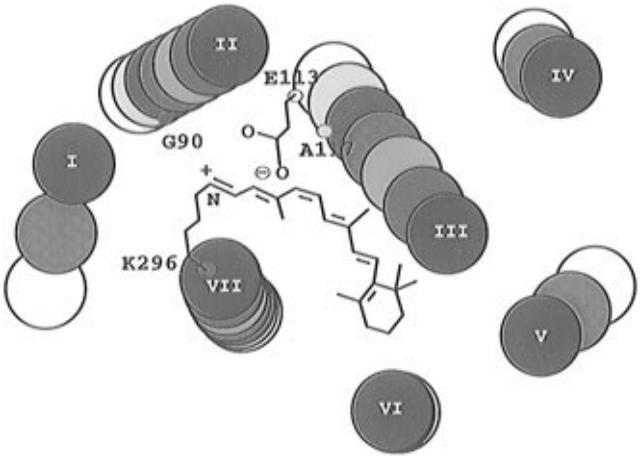

FIGURE 1: Projection model of bovine rhodopsin adapted from Baldwin (1993). Each different color represents a helix turn in the seven TM helices. The view is from the cytoplasmic side (dark blue level) to the intradiscal side (white level) of the receptor. The membrane plane is the plane of the paper. Glu^{113} (white level) points up and Lys^{296} (green level) points down. Ala^{117} is located at the yellow level and in the mutant E113A/A117E Glu^{117} points down. Gly^{90} is located between the yellow and orange levels. 11-*cis*-Retinal is twisted approximately 30° at single bonds C_6-C_7 and $C_{12}-C_{13}$ each to overcome steric hindrance of Me groups with adjacent hydrogen atoms. In addition, the retinal is tilted (with the retinal plane defined as C_7-C_{12}) approximately 20° (ring portion pointing up) to account for the 16° angle of the pigment transition dipole moment relative to the membrane plane. The arrangements of TM helices 3 and 5 have been changed to account for the most recent data presented by Schertler and Hargrave (1995), which tilt TM helix 3 more so that it comes closer to the top region of TM helix 5.

Scheme 1

$$\text{rho} \xrightarrow{h\nu} \text{batho} \rightarrow \text{lumi} \rightarrow ...$$

the mechanism revealed in room temperature experiments is

Scheme 2

$$\text{rho} \xrightarrow{h\nu} \text{batho} \rightleftharpoons \text{bsi} \rightarrow \text{lumi} \rightarrow ...$$

The intermediate bsi was originally observed in low-temperature trapping experiments on an artificial pigment (Shichida et al., 1981). In that work the equilibrated mixture which was trapped was named BL. It is difficult to study the bsi intermediate with steady-state techniques since it has not been directly observed in native rho at low temperatures where it might be stable. Thus, evidence from vibrational spectroscopies about the nature of bsi have come from studies of artificial pigments in which the bsi intermediate is stabilized relative to batho. Nevertheless, such studies show largely reduced HOOP modes, indicating that the twists of the chromophore have relaxed (Ganter et al., 1991). In addition, the altered C=N stretch and deuterium-induced downshift in bsi give evidence for a changed SB environment in this intermediate (Ganter et al., 1991). The decay of bsi results in the formation of lumi, which is characterized by low HOOP intensities and small deuterium-induced downshift of the SB, as in bsi. However, stronger intensities of the amide I bands and bands caused by Glu^{122} show that in lumi the protein is distorted to a larger degree than in bsi (Siebert, 1995).

Although much information about these early stages in signal transduction of rhodopsin has been obtained from low-temperature trapping experiments, information about the nature of the bsi intermediate as well as information about the early photolysis reaction kinetics must come from studies carried out under more physiologically relevant temperature conditions. For example, chromophoric structural characteristics of early intermediates of rho have been deduced from studies of a series of artificial rhodopsins in which the natural retinal chromophore was replaced with synthetic retinals modified to test the effects of various retinal structural features (Kliger & Lewis, 1995; Imamoto et al., 1996). However, time-resolved spectral studies of rhodopsin mutants have until now been impractical because rho mutants have been available only in quantities of the order of a few hundred micrograms. It was impossible previously to obtain nanosecond time-resolved spectra of such small quantities of photolabile materials with sufficient signal to noise to extract useful spectral and kinetic data. Recently, however, we developed a method that makes it possible to measure spectra with 20 ns time resolution on photolabile samples as small as 1 μL (Lewis & Kliger, 1993). In this paper, we apply this system to time-resolved UV−visible spectroscopic measurements of recombinant rhodopsin and rhodopsin mutants using quantities as small as 300 μg. This allows us to determine reaction schemes, including decay constants and λ_{max} values of their photointermediates. We chose to look at mutants in which the protonated Schiff base counterion, Glu^{113}, is replaced in a way that should allow the effects of varying protonated Schiff base−counterion distance to be probed. Since the spectra of retinal proteins are known to be strongly affected by this distance, we hoped to be able to obtain new structural information about rhodopsin photointermediates from the study of these mutants. Figure 1 shows the positions of the various counterion replacement residues studied. In mutant E113D, Glu^{113} is replaced with the smaller aspartic acid residue, thus increasing the chromophore−counterion distance. In mutant E113A/A117E, the counterion moves farther toward the protein center. In mutant G90D, placement of an aspartic acid at position 90 results in introduction of a potential counterion in TM helix 2, since Glu^{113} gets protonated upon incorporation of the Asp at position 90 (Fahmy et al., 1996; Zvyaga et al., 1996). In addition to obtaining information about spectral shifts of photointermediates in the different mutants, dramatic effects of these mutations on the kinetics of the photointermediates were found. These observations, together with previous FTIR measurements of these mutants, provide insights into the structures of photointermediates and the barriers affecting their transformations.

MATERIALS AND METHODS

Preparation of Rhodopsin Mutants. Site-directed mutagenesis of bovine opsin was carried out as previously reported for mutants E113D (Sakmar et al., 1989), E113A/A117E (Zvyaga et al., 1994), and G90D (Zvyaga et al., 1996). Opsin genes were expressed in COS-1 cells and reconstituted with 11-*cis*-retinal. The resulting pigments were purified in dodecyl maltoside buffer solution [10 mM Tris-HCl, pH 7.0, 30 mM NaCl, 60 mM KCl, 2 mM $MgCl_2$, 0.1% (w/v) dodecyl maltoside] and concentrated as described previously (Fahmy & Sakmar, 1993; Zvyaga et al., 1994).

The amounts and concentrations of the samples were as follows: COS-cell rho, 450 μL of 0.69 mg/mL; E113D, 450 μL of 0.69 mg/mL; E113A/A117E, 700 μL of 0.67 mg/mL; G90D, 1300 μL of 0.23 mg/mL.

Time-Resolved Spectroscopy. All laser photolysis measurements were performed in a microapparatus described previously (Lewis & Kliger, 1993). One microliter aliquots of pigment solution were photolyzed by 7 ns (fwhm), 80 μJ/mm^2 pulses of 477 nm light from a Quanta Ray DCR-2 Nd:YAG pumped dye laser. The laser beam entered the sample at an angle of 90° from the probe beam, with vertical polarization. The probe beam polarization axis was set at magic angle (54.7°) with respect to the laser beam polarization to avoid kinetic artifacts due to rotational diffusion. The probe beam path length through the sample was 2 mm. After each laser pulse, the 1 μL sample was replaced by a flow system using a syringe whose plunger was controlled by a computer-driven stepper motor. Difference spectra were measured with a gated (20 ns) optical multichannel analyzer system as described previously (Einterz et al., 1987; Lewis et al., 1987). In order to determine absolute spectra of the photolysis intermediates, a photobleaching difference spectrum, from which the amount of rhodopsin bleached and the amount isorhodopsin formed by each laser pulse could be calculated, was obtained as described previously (Albeck et al., 1989).

Time-resolved spectral measurements were carried out at 20 °C for rho and mutant pigment E113D and at 10 °C for mutant pigments G90D and E113A/A117E. The latter two mutants were studied at lower temperature because at 20 °C most of the batho intermediate already had decayed at the first time point investigated (20 ns).

Data Analysis. The data were analyzed using global exponential fitting following singular value decomposition (SVD) as described elsewhere (Thorgeirsson et al., 1993; Hug et al., 1990). This procedure fits the entire set of absorbance data at all wavelengths and delay times simultaneously. In this section, as an example of all data analysis, we demonstrate the method using the set for COS-cell rho taken at early times: 30, 60, 120, 240, 480, and 960 ns after photolysis (Figure 2a).

In the fitting procedure the best fit was taken to be the one with the smallest number of exponentials giving reasonable residuals (actual data minus fit). In the case of rho at early times the best fit was a two-exponential fit with time constants $\tau_1 = 30$ ns and $\tau_2 = 244$ ns. The corresponding amplitudes, called b-spectra (in the following we refer to "experimental" b-spectra to distinguish them from the calculated b-spectra determined at a later fitting step), are shown in Figure 2b (colored spectra) together with the residuals (Figure 2c). The b_0 curve is the time-independent b-spectrum.

The next step in the analysis is to propose a kinetic scheme which can explain the time evolution of the absorption difference spectra and which agrees with the two-exponential fit. The final goal is to obtain the pure intermediate spectra. Because there is no clear isosbestic point in the set of difference spectra and two-exponential time constants were required to fit the data, more than two intermediates are needed to explain the time evolution of the spectra (Hug et al., 1990). The kinetic scheme that best fit the rho data was the one previously established (Scheme 2).

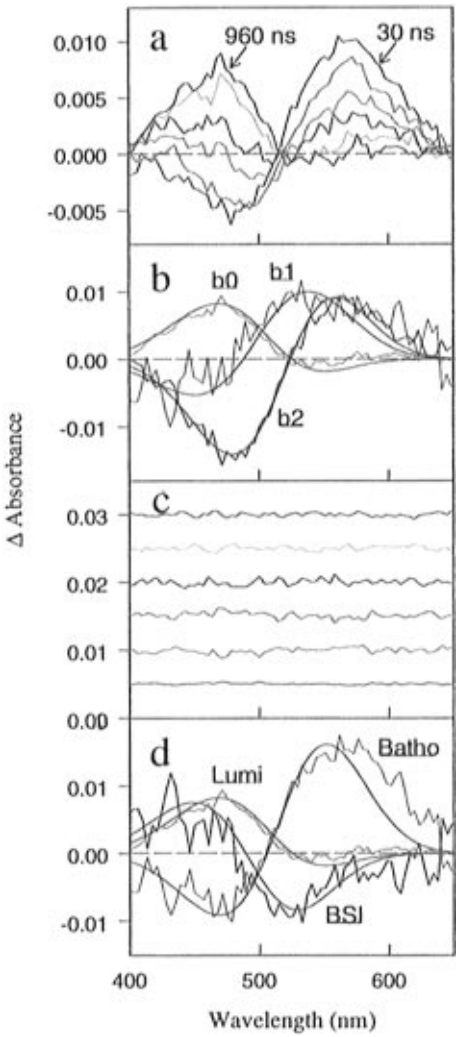

FIGURE 2: (a) Difference spectra for COS-cell expressed rho solubilized in dodecyl maltoside after photolysis with 7 ns (fwhm) 477 nm laser pulses at 20 °C, pH 7. Spectra were collected at 30, 60, 120, 240, 480, and 960 ns after photolysis. The lack of an isosbestic point indicates that there are more than two intermediates involved. (b) Experimental b-spectra resulting from a two-exponential fit (colored curves). The corresponding decay times are $\tau_1 = 30$ ns and $\tau_2 = 244$ ns. Based on five independent experiments with comparable amounts of rhodopsin solubilized in detergent and measured under identical conditions, τ_1 can differ by a factor of up to 2 and τ_2 can differ by a factor of up to 1.5 (data not shown). b_0 is the time-independent spectrum (green curve). The black curves are calculated b-spectra using the proposed intermediate − bleach spectra and the optimized kinetic matrix (see Data Analysis in Materials and Methods). (c) Residuals resulting from the two-exponential fit (actual data minus two-exponential fit). They are shown from the bottom to the top in order of increasing time. (d) Experimental intermediate − bleach spectra (noisy colored curves) calculated from the experimental b-spectra (panel b) and the kinetic matrix. The proposed intermediate − bleach spectra are shown as solid black curves. See also Data Analysis in Materials and Methods. The λ_{max} values and the decay constants from the fit are summarized in Tables 1 and 2. Estimated errors for λ_{max} values are ±2 nm.

In the fitting procedure we followed a method similar to the algebraic method described by Thorgeirsson et al. (1993), because it allows more complex schemes to be fit. The b-spectra determined from the global exponential fit are connected to the eigenvectors, $\mathbf{V}_i$, of the kinetic matrix and can be written as column vectors $\mathbf{b}_i$:

$$\mathbf{b}_i = \epsilon(\lambda) f_i \mathbf{V}_i \qquad (1)$$

for the *i*th state with nonzero decay constant, and as

$$\mathbf{b}_0 = \epsilon(\lambda)(f_0\mathbf{V}_0 - \mathbf{c}_{bl}) \quad (2)$$

for the time-independent state. Here $\epsilon(\lambda)$ is a matrix containing wavelength-dependent extinction values of the intermediate spectra as column vectors, $\mathbf{V}_i$ is the eigenvector of the kinetic matrix arranged as a column vector, f_i are scalar factors to satisfy the conditions at time 0, and $\mathbf{c}_{bl}$ represents the bleach written as a column vector. For the calculations involved in the fitting procedure the b-spectra are arranged in an $m \times (k + 1)$ matrix with m the number of wavelengths measured and k the number of exponentials. The intermediate − bleach spectra are in an $m \times n$ matrix with n the number of intermediates. Initially, for the intermediate − bleach spectra, the λ_{max} values, extinction coefficients, and skewed Gaussian parameters of the intermediates have to be guessed. Therefore, we refer to them as "proposed" intermediate − bleach spectra. Once the skewed Gaussian parameters have been established, they were kept unchanged throughout the fitting procedure. We were able to use the skewed Gaussian forms derived for rho for all the mutants investigated. The λ_{max} values and values for the extinction coefficients for each intermediate were the variable parameters during the fitting procedure.

The kinetic matrix contains the information about the kinetic scheme. Once a scheme was chosen by restricting certain kinetic matrix elements to be zero, the fitting procedure optimized the microscopic rate constants to satisfy the proposed intermediate − bleach spectra. If the chosen scheme produced a reasonable fit to the b-spectra, the parameters (λ_{max} values and values for the extinction coefficients of the proposed intermediate − bleach spectra) were fine tuned, and the fit was further optimized. The experimental b-spectra, which were obtained before choosing a kinetic scheme, and the b-spectra calculated from eqs 1 and 2 (*i.e.*, from the proposed intermediate − bleach spectra and the optimized kinetic matrix) are shown for rho in Figure 2b as colored lines and black lines, respectively. We refer to the b-spectra calculated from eqs 1 and 2 as "calculated" b-spectra. To verify the validity of the fit, the experimental b-spectra and the fitted kinetic matrix were used to calculate the experimental intermediate − bleach spectra (colored lines) shown in Figure 2d together with the proposed intermediate − bleach (black lines) spectra. Experience with the fitting procedure has shown that comparison of the proposed and the experimental intermediate − bleach spectra is a more sensitive test for the quality of the fit than is the fit to the b-spectra.

For the two mutants E113A/A117E and G90D an additional procedure preceded the fitting. Adding back the bleach to the 20 ns difference spectrum results in a very broad spectrum with half-width values (fwhm) of ≈200 nm compared to ≈120 nm found for the batho and bsi spectra of rho and E113D (data not shown). Therefore, the 20 ns difference spectrum was taken to represent a batho/bsi mixture. The relative amounts of batho and bsi were calculated from the decomposition of the 20 ns difference spectrum by guessing the λ_{max} values as well as the relative amounts of both intermediates present 20 ns after photolysis. Once a reasonable decomposition was found, these values were used to continue the fitting procedure as described above. Both procedures were applied several times until the fit was optimized. For both mutants, 55% batho and 45% bsi in the 20 ns mixture gave the best fits. The error bounds for the relative amounts in E113A/A117E and in G90D were 10% and 20%, respectively. The larger error for mutant G90D is due to the reduced red shift of G90D batho.

Table 1: Summary of the λ_{max} Values[a,c] (in nm) of the Intermediates of the Three Counterion Mutants, COS-Cell Rhodopsin, and Rhodopsin[b]

species	rhodopsin[b]	COS rho	E113D	E113A/A117E	G90D
pigment	498	500	509	490	484
batho	529 (+31)	531 (+31)	540 (+31)	525 (+35)	500 (+16)
bsi	477 (−21)	479 (−21)	495 (−14)	453 (−37)	440 (−44)
lumi	492 (−6)	490 (−10)	486 (−23)	482 (−8)	479 (−5)
MI	n/a	n/a	n/a	466 (MI-like)	460 (MI-like)
MII	380	380	380	380 (MII-like)	380 (MII-like)

[a] The estimated errors of λ_{max} values are ±2 nm, except for E113A/A117E- and G90D-batho and bsi where they are ±4 nm. [b] Values from Hug et al. (1990). [c] Values in parentheses are spectral shifts of the intermediates relative to the dark state parent pigment spectra.

RESULTS

Rhodopsin mutants E113D, E113A/A117E, and G90D were constructed by site-directed mutagenesis, expressed, regenerated with 11-*cis*-retinal, and purified in detergent solution for spectral analysis. The λ_{max} values of the dark states of the mutant pigments are listed in Table 1 [taken from Zvyaga et al. (1993, 1996)]. Figure 3 shows the time-dependent absorption difference spectra of rho (Figure 3a) and the mutants E113D (Figure 3b), E113A/A117E (Figure 3c), and G90D (Figure 3d). At early times following photolysis, the difference spectra clearly show the presence of batho for rho and E113D and, to a reduced extent, for E113A/A117E and G90D. For the latter two mutants, our time resolution of 20 ns was not fast enough to resolve the batho to bsi transition kinetics. While the apparent rates and b-spectra are adequate for qualitative understanding of the processes taking place, more detailed analysis has to be employed to obtain microscopic rates and intermediate spectra. This involved using a global exponential fitting procedure following singular value decomposition (SVD) described elsewhere (Thorgeirsson et al., 1993; Hug et al., 1990), with an extended fitting procedure as described in Materials and Methods.

COS-Cell Rho. Data analysis was carried out on data from early times, 30−960 ns (see Materials and Methods). The microscopic rate constants as well as the λ_{max} values of the intermediates are in excellent agreement with data obtained from detergent-solubilized rod outer segment (ROS) rhodopsin (Hug et al., 1990). The earlier λ_{max} values and time constants were compared to the values obtained in this study and are listed in Tables 1 and 2, respectively. The results demonstrate that time-resolved UV−visible spectroscopy can be performed on samples as small as 300 μg (used in this experiment). Employing the entire time range (30 ns−10 ms) gives three exponentials with time constants $\tau_1 = 57$ ns, $\tau_2 = 320$ ns, and $\tau_3 = 308$ μs. The corresponding b-spectra are shown in Figure 4a ($b_1 = 57$ ns, $b_2 = 320$ ns, $b_3 = 308$ μs; b_0 is the time-independent spectrum), and the residuals of the fit (actual data − three-exponential fit) are shown in Figure 4b. Only the following scheme could fit

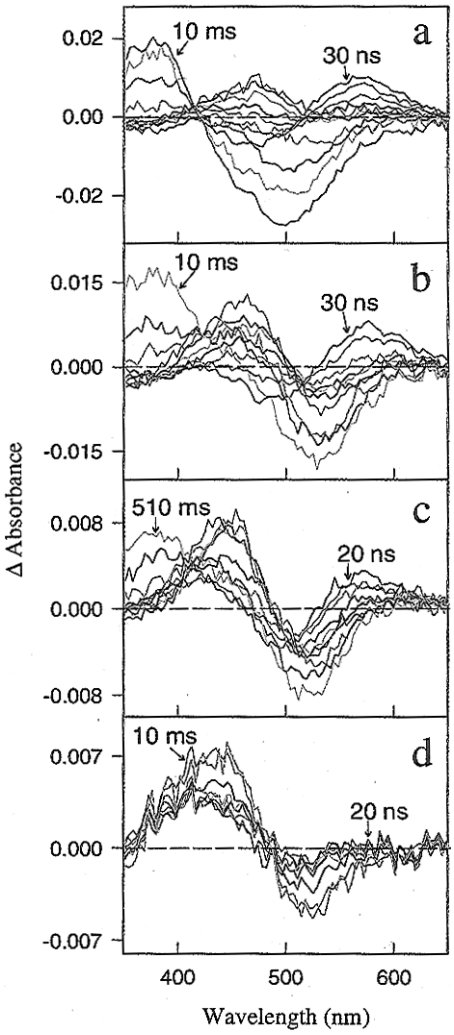

FIGURE 3: (a) Difference spectra for rho as in Figure 2a with late time points 10, 100, 250, and 500 μs and 10 ms included. Measuring conditions (T = 20 °C) were unchanged during the entire time range. (b) Difference spectra for mutant E113D measured under identical conditions as for rho (see Figure 2a and panel a of this figure). Difference spectra after 960 ns were collected at 50, 250, and 500 μs and 10 ms after photolysis. The region of the overlapping spectra in the time interval 30−960 ns is clearly different from that of rho. (c) Difference spectra for mutant E113A/A117E as measured for rho (see panel a) but at T = 10 °C. The time-dependent difference spectra are considerably different when compared to rho. Difference spectra were collected at 20, 60, 200, and 800 ns, 3, 10, and 50 μs, and 1, 10, and 510 ms after photolysis. The first spectrum at 20 ns already contains substantial amounts of bsi. T = 10 °C was chosen because at T = 20 °C the batho amplitude at 20 ns was very small, most likely because more batho had already decayed at the earliest time point collected at 20 °C (data not shown). (d) Difference spectra for mutant G90D measured under identical conditions as for E113A/A117E. Difference spectra were collected at 20, 60, 200, and 800 ns, 3, 10, and 50 μs, and 10 ms after photolysis. Due to a less pronounced batho red shift, the batho component is hidden in the bleach part of the difference spectrum.

the whole data set:

Scheme 3a

$$\text{batho} \rightleftharpoons \text{bsi} \rightarrow \text{lumi} \rightarrow \text{MII} \rightarrow ...$$

resulting in intermediate − bleach spectra shown in Figure 4c. We were unable to find a scheme that included a MI-like absorber, confirming the observation that no MI photoproduct is found in dodecyl maltoside-solubilized rhodopsin above freezing (Franke et al., 1992). The fact that no MI was observed in the detergent-solubilized sample shows that the pigment (in detergent) strongly prefers a deprotonated SB environment after lumi. In Figure 4d the bleach was added back to the intermediate − bleach spectra showing the pure intermediate spectra. Since the MII spectrum showed the same 380 nm absorption features for rho and for all mutants investigated, we did not include them in Figures 4−7, panels d. The kinetic and spectral results are summarized in Tables 1 and 2.

Mutant Pigment E113D. Replacing the Glu^{113} counterion by the shorter Asp residue results in a red shift of the pigment spectrum of about 10 nm (Sakmar et al., 1989; Zvyaga et al., 1993; Table 1). This is consistent with an increased distance of the counterion from the SB proton and implies that the counterion chain points in the general direction of the SB (Figure 1). Figure 3b shows the difference spectra for times from 30 ns to 10 ms after photolysis. Analyzing the early times from 30 to 960 ns results in Scheme 2, as observed for rho. When times up to 10 ms are included in the analysis, we obtained a three-exponential fit with time constants τ_1 = 72 ns, τ_2 = 935 ns, and τ_3 = 590 μs. The corresponding b-spectra and the residuals are shown in panels a and b of Figures 5, respectively. No scheme other than Scheme 3b, which included a lumi ← MII back-reaction, could fit the whole data set:

Scheme 3b

$$\text{batho} \rightleftharpoons \text{bsi} \rightarrow \text{lumi} \rightleftharpoons \text{MII} \rightarrow ...$$

Obviously the shortening of the counterion side chain has an influence on the Schiff base deprotonation reaction.

Comparing the microscopic lifetimes of E113D to rho (Table 2), the batho ⇌ bsi equilibrium is forward shifted and the later reactions are slowed down by a factor of 3−4 ($\approx 2k_bT$, which is small compared to the ΔG values involved in the transitions of the intermediates). Figure 5c shows the intermediate − bleach spectra resulting from Scheme 3b, and Figure 5d shows the pure intermediates with bleach added back. Tables 1 and 2 summarize the results. Although E113D batho shows an identical spectral red shift relative to its parent pigment compared to that of rho, the subsequent E113D intermediates are shifted differently: bsi is blue shifted by only 14 nm and lumi is blue shifted by 23 nm (bsi and lumi are 21 and 10 nm blue shifted, respectively, in rho). Finally lumi decays to MII, which absorbs at 380 nm in rho and in all mutants. The main difference between the E113D mutant and rho in MII kinetics is the existence of a lumi ← MII back-reaction. Even in detergent the final product is a mixture of protonated and deprotonated forms.

Mutant Pigment E113A/A117E. In this mutant the counterion is moved one helix turn (four side chain positions ≈ 5.4 Å, 400°) toward the center of the membrane-embedded domain. This places the counterion closer to the SB, as indicated by a 10 nm blue shift of the pigment spectrum (Zvyaga et al., 1993, 1994; Table 2). Figure 3c shows the difference spectra from 20 ns to 510 ms after photolysis. The first difference spectrum at 20 ns clearly results from more than one intermediate. This means that the first time constant (batho decay into equilibrium with bsi) cannot be resolved and is thus faster than 20 ns. Analyzing the 20 ns to 50 μs data results in a two-exponential fit with time constants τ_1 = 78 ns and τ_2 = 1.5 μs. The data could be fit

Table 2: Summary of the Decay Times[a] of the Intermediates of the Three Counterion Mutants, COS Cell Rhodopsin, and Rhodopsin[b]

species	rhodopsin[b] (T = 12 °C)	COS rho (T = 20 °C)	E113D (T = 20 °C)	E113A/A117E (T = 10 °C)	G90D (T = 10 °C)
batho → bsi	120 ns	100 ns	90 ns	<20 ns	<20 ns
bsi → batho	160 ns	190 ns	440 ns		
bsi → lumi	150 ns	190 ns	750 ns	190 ns	200 ns
lumi → bsi	none	none	none	210 ns	170 ns
lumi → MI-like				2.0 ms	9.3 ms
MI-like → lumi				2.9 ms	none
lumi → MII	600 μs	310 μs	1.0 ms		
MII → lumi	none	none	1.4 ms		
MI-like → MII-like				11.8 ms	not measured
MII-like → MI-like				9.9 ms	

[a] The estimated errors of the decay times are 20%. [b] Values from Hug et al. (1990).

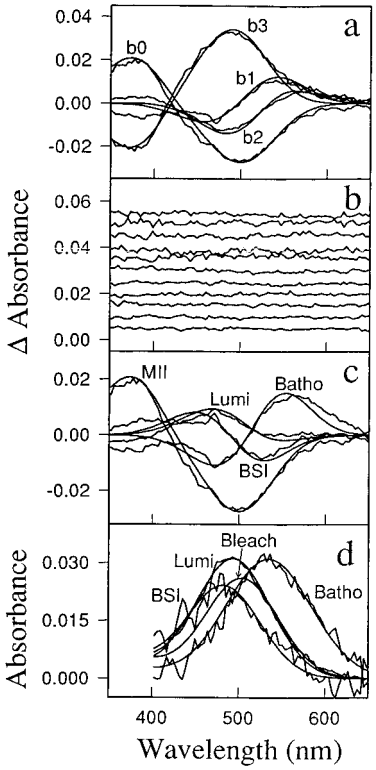

FIGURE 4: Data analysis for rho. (a) Experimental b-spectra resulting from a three-exponential fit (noisy curves). The corresponding decay times are τ_1 = 57 ns, τ_2 = 320 ns, and τ_3 = 308 μs. The solid curves are calculated b-spectra (see Materials and Methods). (b) Residuals from the three-exponential fit (actual data minus three-exponential fit). From 30 to 960 ns more data were collected (nine difference spectra for each time point) than from 10 μs to 10 ms (two to three difference spectra each), which accounts for the larger residuals at later times shown in the upper part of the panel. (c) Experimental intermediate − bleach spectra (noisy curves) and proposed intermediate − bleach spectra (smooth curves) (see Materials and Methods for the calculations). (d) Bleach added back to the intermediate − bleach spectra of panel c, resulting in the pure intermediates. The λ_{max} values and the decay constants from the fit are summarized in Tables 1 and 2. Estimated errors for λ_{max} values are ±2 nm.

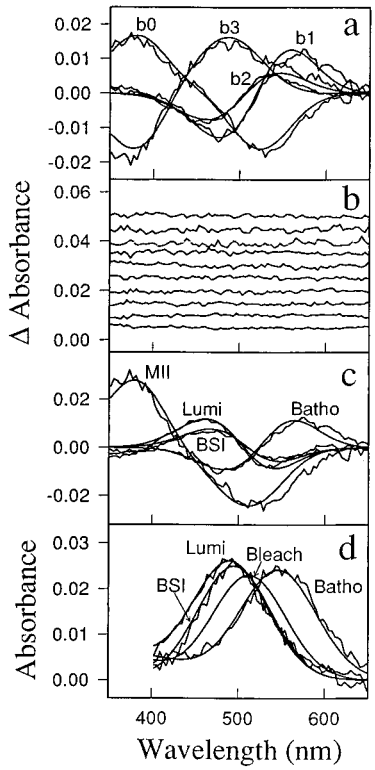

FIGURE 5: Data analysis for mutant pigment E113D. (a) Experimental b-spectra resulting from a three-exponential fit. The corresponding decay times are τ_1 = 72 ns, τ_2 = 935 ns, and τ_3 = 590 μs. The solid curves are calculated b-spectra. (b) Residuals from the three-exponential fit. From 30 to 960 ns, six to eight difference spectra and, from 50 μs to 10 ms, two difference spectra at each time point were collected. As a result the late times have noisier residuals (upper part of the panel). (c) Experimental intermediate − bleach spectra (noisy curves) and proposed intermediate − bleach spectra (smooth curves) (see Materials and Methods for the calculations). (d) Bleach added back to the intermediate − bleach spectra of panel c, resulting in pure E113D intermediates. The λ_{max} values and the decay constants from the fit are summarized in Tables 1 and 2. Error bounds are the same as for rho.

best to the following scheme:

Scheme 4a

$$\text{batho/bsi} \rightleftharpoons \text{lumi} \rightleftharpoons \text{MI-like (R*)} \rightarrow ...$$

Employing the entire 20 ns−510 ms time range results in a three-exponential fit with time constants τ_1 = 96 ns, τ_2 = 1.7 μs, and τ_3 = 7.2 ms. The corresponding b-spectra and residuals are shown in panels a and b of Figure 6, respectively. To satisfy the fitting procedure for all times, a spectrally MII-like species (λ_{max} = 380 nm) has to be included in an extended Scheme 4a:

Scheme 5

$$\text{batho/bsi} \rightleftharpoons \text{lumi} \rightleftharpoons \text{MI-like (R*)} \rightleftharpoons \text{MII-like} \rightarrow ...$$

The intermediate − bleach spectra resulting from this scheme are shown in Figure 6c. Adding back the bleach gives the

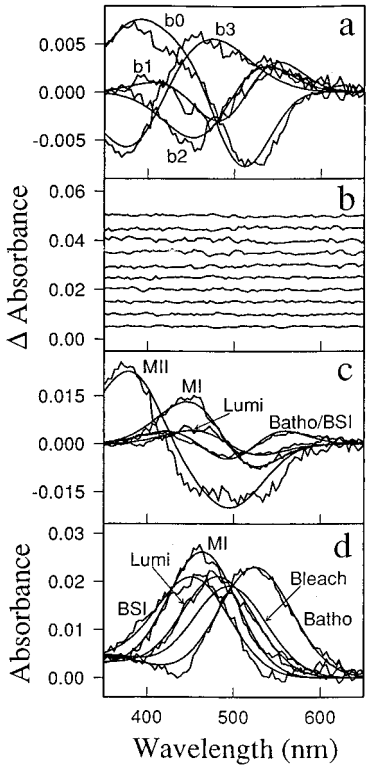

FIGURE 6: Data analysis for mutant pigment E113A/A117E. (a) Experimental b-spectra resulting from a three-exponential fit. Because the batho to bsi transition was too fast to resolve, τ_1 describes the decay of the batho/bsi mixture. The decay times are $\tau_1 = 96$ ns, $\tau_2 = 1.7$ μs, and $\tau_3 = 7.2$ ms. The smooth curves are calculated b-spectra. (b) Residuals from the fit. From 20 ns to 3 μs, eight difference spectra, at 10 μs, six difference spectra, and from 50 μs to 510 ms, three difference spectra were collected at each time point, which leads to noisier residuals for the late times (upper part of the panel). (c) Experimental (noisy curves) and proposed (smooth curves) intermediates − bleach spectra. (d) Bleach added back to the intermediate − bleach spectra of panel c. The λ_{max} values and kinetics are summarized in Tables 1 and 2. Estimated errors for λ_{max} values are ±2 nm except for batho and bsi. Because the initial concentrations present in the 20 ns difference spectrum have higher error bounds, the λ_{max} values are ±4 nm for batho and bsi.

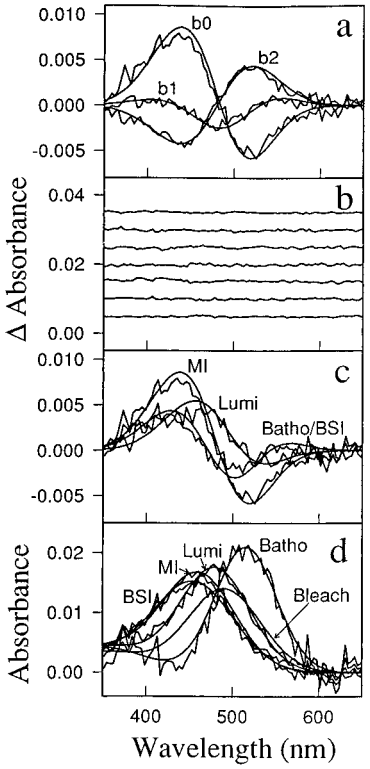

FIGURE 7: Data analysis for mutant pigment G90D. (a) Experimental b-spectra resulting from a two-exponential fit. The corresponding decay times are $\tau_1 = 91$ ns and $\tau_2 = 20.4$ μs. The solid curves are calculated b-spectra. (b) Residuals from the fit. From 20 ns to 50 μs, 16 difference spectra and, at 10 ms, 2 difference spectra were collected at each time point. (c) Experimental (noisy curves) and proposed (smooth curves) intermediates − bleach spectra. (d) Bleach added back to the intermediate − bleach spectra of panel c. The λ_{max} values and kinetics are summarized in Tables 1 and 2. Error bounds are the same as for mutant E113A/A117E.

pure intermediate spectra (Figure 6d). All data are summarized in Tables 1 and 2.

A slightly increased batho red shift (35 nm relative to 31 nm for rho) is followed by a blue shift of 37 nm in bsi, which is substantially more than that observed for rho (21 nm). For the next intermediate, lumi, the blue shift (8 nm relative to the ground state) is similar to that of rho. Comparing the kinetics of E113A/A117E with rho, the batho → bsi transition has speeded up substantially (<20 ns). Surprisingly, in this mutant a spectrally MI-like absorber could be distinguished from a spectrally MII-like absorber. However, it was shown that this MI-like absorber ($\lambda_{max} = 466$ nm) has conformational features of MII as detected by FTIR (Fahmy et al., 1994) and represents the transducin-activating species (Zvyaga et al., 1994). Therefore, we refer to the MI-like species as R*. Whether the "MII-like" absorber still represents a SB linkage or is already free *all-trans*-retinal + opsin (Zvyaga et al., 1996) cannot be determined at this point. The latter case, however, would imply that free *all-trans*-retinal is able to rebind covalently to Lys[296] since there exists a MI-like ← MII-like back-reaction. The ability of mutant opsins to bind free *all-trans*-retinal to Lys[296] has been shown for E113Q (Sakmar et al., 1989).

The most striking feature of Scheme 5 is that all intermediates are in equilibrium, showing that the pigment does not prefer the protonated to the deprotonated SB environment and that the product at any time point is a mixture of all intermediates which have formed up to that time.

Mutant Pigment G90D. In the mutant G90D a new potential counterion (Asp) was introduced in TM helix 2 at position 90, which is able to substitute for Glu[113] as the SB counterion (Rao et al., 1994; Zvyaga et al., 1996; Fahmy et al., 1996; see Discussion). Figure 3d shows the difference spectra from 20 ns to 10 ms after photolysis. The first difference spectrum at 20 ns again clearly shows the presence of more than one intermediate, as was also the case for mutant E113A/A117E. The presence of bsi now is more evident than batho at this time since, as shown by the data analysis, batho is less red shifted than usual and therefore hidden in the bleach. Analyzing the whole data set results in a two-exponential fit with time constants $\tau_1 = 91$ ns and $\tau_2 = 20.4$ μs. The corresponding b-spectra and residuals are shown in panels a and b of Figure 7, respectively. The best fit was given by Scheme 4b:

Scheme 4b

$$\text{batho/bsi} \rightleftharpoons \text{lumi} \rightarrow \text{MI-like (R*)} \rightarrow \ldots$$

Again, batho decay was too fast to resolve (<20 ns). As with mutant E113A/A117E, the best fits were obtained by

assuming a batho/bsi mixture decaying to lumi, which decays to a MI-like absorber. No lumi ← MI-like back-reaction was observed for mutant G90D, in contrast to mutant E113A/A117E (Scheme 4a). The intermediate − bleach spectra are shown in Figure 7c, and the pure spectra of the intermediates with bleach added back are shown in Figure 7d. All data are summarized in Tables 1 and 2.

The kinetics of mutant G90D and of mutant E113A/A117E are very similar except for the absence of the lumi ← MI-like back-reaction in the G90D mutant. However, the λ_{max} values for the intermediates of the two mutants differ. The batho red shift is less pronounced in G90D (16 nm), as was observed in an FTIR and UV−visible study at low temperature (Fahmy et al., 1996), and bsi shows a pronounced blue shift (44 nm). In lumi, the blue shift (5 nm) is comparable to those of mutant E113A/A117E and rho.

DISCUSSION

In this study we demonstrate the utility of investigating recombinant visual pigments by time-resolved UV−visible spectroscopy, focusing on a set of three mutant pigments in which the SB counterion environment has been altered (E113D, E113A/A117E, and G90D). The results of these studies are reconciled with existing information from a variety of sources as discussed below.

Mutant Pigment E113D. In mutant E113D, Glu^{113} was replaced by an Asp residue, which has a shorter side chain. Investigating the early times up to 1 μs shows that after photolysis the reaction follows the scheme established for the native pigment (Scheme 2). Obviously the slightly increased distance of the counterion from the chromophore only mildly affects the transitions of the early intermediates. This correlates nicely with an FTIR study where the 1238 cm^{-1} band, which has been described as a coupling of C_{12}−C_{13}, C_{14}−C_{15} stretching vibrations and NH, C_{14}−H, and C_{15}−H bending vibrations (Palings et al., 1987; Ganter et al., 1988a,b) was unaffected by this mutation (Jäger et al., 1994). Furthermore, the entire chromophore "fingerprint region" of mutant E113D between 1200 and 1300 cm^{-1}, which is characteristic of retinal geometry, was reported to be very similar to that of rho (Jäger et al., 1994). In addition, the batho red shift is identical to that of rho (Table 1). In an NMR study of the native pigment this red shift could be accounted for by two effects: (1) twisting of the chromophore and (2) a change in orientation of the negative charge of the counterion relative to the retinal plane, the two being in-plane in batho of the native pigment (Han & Smith, 1995). Because retinal geometry in the parent pigments, as well as batho decay times, is very similar between E113D and rho, it is reasonable to assume that the twisting of the chromophore is the same in batho and E113D batho and that Asp^{113} in E113D batho is probably located at a similar angle to the plane of the retinal, as is Glu^{113} in the native pigment.

It is known that the electrostatic environment of the protonated SB is an important determinant of the visible absorption maximum (Blatz et al., 1972; Honig et al., 1976, 1979; Kliger et al., 1977; Arnaboldi et al., 1979; Koutalos et al., 1989; Birge, 1988, 1990). Therefore, comparing the spectra of different mutants to that of rho gives an estimate for the counterion−protonated SB distance. In batho, newly introduced twists of the retinal, in addition to isomerization, contribute to the visible absorption maximum. This usually complicates calculations about the counterion−protonated SB distance from the UV−visible data in batho, unless other information from NMR, Raman, or FTIR experiments is available. In bsi and lumi the chromophore twists are mainly relaxed. However, additional factors now contribute to the wavelength shifts, and only to the degree that these factors are the same in rho and the mutants studied can shifts in λ_{max} be interpreted in terms of counterion−protonated SB distance.

In spite of the complexity of factors causing the blue shifts of bsi and lumi in rho and in all mutants investigated, inspection of Table 1 reveals a relatively straightforward relationship. Relative to the blue shifts of the intermediates in the native pigment, the blue shift of E113D bsi (14 nm) is smaller, and that of E113A/A117E bsi (37 nm) is larger than native bsi (21 nm), that of E113D lumi is larger (23 nm), and that of E113A/A117E lumi is smaller (8 nm) than native lumi (10 nm). Since the counterions of both mutants and rho are located in the same helix, we assume that the blue shifts of bsi and lumi can be accounted for by the SB−counterion distance. The movement of the SB thus consists of a motion toward Glu^{117} in the transition to bsi and toward Asp^{113} in the transition to lumi. This motion is in agreement with a study on transition dipole orientations in the early photolysis intermediates of rhodopsin (Lewis et al., 1989). The blue shifts and the transition dipole orientations of the intermediates together can be used to deduce chromophore motions in the early intermediates (S. Jäger, J. W. Lewis, T. A. Zvyaga, I Szundi, T. P. Sakmar, and D. S. Kliger, unpublished results).

The λ_{max} values of lumi for COS rho and mutant E113D decrease in going from COS rho (490 nm) to E113D (486 nm) (Table 1). The transition from lumi to MII slows down from 310 μs (COS rho) to 1.0 ms (E113D) (Table 2). It has been proposed that in the transition to MII the SB is exposed to a more hydrophobic protein environment, thus enabling the SB deprotonation (Jäger et al., 1994). We suggest that, in mutant E113D, the closer proximity of Asp^{113} to the SB in E113D lumi provides a stronger stabilizing electrostatic interaction which could not fully be overcome in the transition to E113D-MII, establishing a lumi ⇌ MII equilibrium and slowing the lumi to MII kinetics. Temperature-dependent measurements would be useful to test this hypothesis.

Mutant Pigment E113A/A117E. The double-replacement mutation has a more dramatic effect on the kinetic scheme than observed for mutant E113D. The early times show significant changes in the difference spectra compared to rho or to E113D. Batho decay is faster than 20 ns, which demonstrates that the chromophore twist in batho is relieved much earlier than in rho or in E113D. It has been shown in an FTIR study that the 1238 cm^{-1} band shifts down by 7 cm^{-1}, revealing a change in perturbation of the chromophore in the dark state of this mutant (Fahmy et al., 1994). By comparing this mode (which is highly delocalized in nature) with the corresponding mode in rhodopsin and other mutants lacking the counterion at position 113 (*e.g.*, E113Q, E113A), it is obvious that removal of the negative charge at position 113 causes downshifts of the 1238 cm^{-1} band by 7−8 cm^{-1} (Jäger et al., 1994; Lin et al., 1992). Thus the electrostatic environment near position 113, which was shown to be close

to C_{13} (Birge et al., 1988; Koutalos et al., 1989) and C_{12} (Han et al., 1993; Han & Smith, 1995) influences the "$C_{12}-C_{13}$" frequency (Zvyaga et al., 1996). Therefore, the 1238 cm^{-1} band seems to be a good marker band for electrostatic influences of the counterion and its environment, especially near $C_{12}-C_{13}$. The absence of a counterion at position 113 is correlated with a reduced electrostatic stabilization of the protonated SB and a weaker protein perturbation near $C_{12}-C_{13}$ (Lin et al., 1992).

We suggest that these two effects influence batho decay, which is speeded up substantially in mutant E113A/A117E (<20 ns). It has been proposed that the batho to bsi transition depends on the ease of the 8-H of the retinal to overcome steric hindrance to pass the 5-Me group, which depends on flexibility of the β-ionone ring (Lewis et al., 1995b; Mah et al., 1995). This, along with the accelerated batho decay, suggests that the repositioned Glu^{117} counterion either supports an electron distribution along the retinal chain which facilitates 8-H passing by the 5-Me group or that Ala^{113} has a reduced steric and/or electrostatic interaction with the retinal chain (probably with the 13-Me group) and accelerates bsi formation similarly to removal of the 13-Me group (Einterz et al., 1990).

Does the repositioned counterion (from 113 to 117) have an influence on the steric trigger of the 9-Me group of the retinal? Recently, it was suggested that the 9-Me group might interact with a conserved glycine at position 121 (one helix turn from position 117) (Han et al., 1996), with the two Gly residues forming a cavity for the 9-Me group. Encroachment of a negative charge into this cavity might influence the steric interaction that the 9-Me group exerts on TM helix 3 and thus represents another possible mechanism for accelerating batho decay, as was observed in an FTIR study on 9-deMe pigment (Ganter et al., 1989).

An accelerated batho decay was also observed in the P521 cone-type visual pigment of the *Gecko gecko* retina (Lewis et al., 1995a) and in the chicken red cone pigment iodopsin (Shichida et al., 1993). Furthermore, the batho/bsi mixture of P521 (and, analogously, the BL intermediate in iodopsin) decayed to lumi and then to a MI-like absorber with kinetics very similar to those of the rhodopsin mutant E113A/A117E investigated in this study. The question arises, does repositioning of the counterion from Glu^{113} to Glu^{117} mimic cone-type pigments in terms of trigger mechanisms leading to the active state? The sequences of gecko P521 and iodopsin have striking similarities. Lys^{296} in rhodopsin has its counterparts in Lys^{311} in P521 and Lys^{309} in iodopsin; Glu^{113} in rhodopsin corresponds to Glu^{128} in P521 and to Glu^{126} in iodopsin (Kojima et al., 1995; Kuwata et al., 1990; Tokunaga et al., 1990). The overall sequence homology in the gecko P521 and iodopsin pigments suggests that they share a similar molecular mechanism to reach the active state. One of the differences from rho are three polar residues, one (Tyr^{274}) located near the counterion and the other two (Ser^{177} and Thr^{282}) located near the ring portion of the chromophore which are thought to tune the absorption maxima in cone-type pigments (Lin et al., 1994). We suggest that the same mechanism (weakening of the electrostatic interaction between the counterion Glu^{126} and the PSB; Lin et al., 1994) caused by the polar residue Tyr^{274} in iodopsin accelerates batho decay in iodopsin observed by Shichida et al. (1993). In that pigment the "marker band" at 1238 cm^{-1} has shifted down by 3 cm^{-1}(Lin et al., 1994), supporting our previous hypothesis that this band is linked to the speed of batho decay. Further support for this hypothesis comes from the fact that in E113D the kinetics of batho decay remains unchanged (Table 2), and the 1238-cm^{-1} band does not shift (Jäger et al., 1994). To prove this hypothesis, further measurements (e.g., E113A) are needed.

The batho red shift in E113A/A117E is slightly increased (by 4 nm) relative to rho, which can be due to altered twists of the chromophore and/or altered orientation of the counterion (Han & Smith, 1995). Since both residues are one helix turn apart from each other (≈5.4 Å, 400°), the orientation of Glu^{117} as compared to Glu^{113} is most likely changed.

Most striking is the appearance of a spectrally MI-like intermediate in E113A/A117E absorbing at 466 nm. Because this intermediate has properties which resemble the MII conformation (Fahmy et al., 1994), we denote it as R* in Schemes 4 and 5. R* is the transducin-activating form (Zvyaga et al., 1994), which decays to a 380 nm absorber denoted as MII-like, because of its absorption at 380 nm. Both forms (protonated and deprotonated) are in equilibrium with each other (Scheme 5). The existence of a back-reaction (deprotonated to protonated form) was also observed in mutant E113D (Table 2). We suggested above that the strong stabilizing electrostatic interaction, due to the decreased counterion−SB distance in the lumi intermediate, could not be fully overcome in the transition to the unprotonated form. The absorption of E113A/A117E lumi (482 nm), which is even more shifted to the blue than E113D lumi (486 nm), argues for the same mechanism in both mutants. The slowed down MI-like to MII-like kinetics again fit into this line of reasoning.

The existence of a back-reaction of MI to lumi has been reported for chicken rhodopsin (Imai et al., 1994). This was explained by a rising ΔG value of MI (compared to lumi) upon warming, showing that entropic processes contribute to the architecture of the kinetic scheme as well. Thermal equilibria among the intermediates lumi, MI, and MII seem to be a common feature in many visual pigments since these equilibria were observed in chicken rhodopsin (Imai et al., 1994) and the cone-type visual pigment gecko P521 (Kojima et al., 1995).

Mutant Pigment G90D. The G90D mutation in human rhodopsin is known to cause congenital night blindness (Rao et al., 1994; Fahmy et al., 1996). The G90D pigment absorption is 16 nm blue shifted relative to native rhodopsin, indicating that in this mutant the counterion (Asp^{90}) may reside closer to the SB than in rho or in the two other mutants studied (Figure 1). Asp^{90} competes with Glu^{113} to be the counterion of the protonated SB (Rao et al., 1994; Zvyaga et al., 1996; Fahmy et al., 1996). Evidence has been presented that Glu^{113} is protonated in the dark state as well as in the photoproduct (Fahmy et al., 1996; Zvyaga et al., 1996), which establishes a new electrostatic interaction between Asp^{90} and the protonated SB. This electrostatic interaction must be very similar to the one obtained by moving the counterion one helix turn toward the cytoplasmic side of the protein (E113A/A117E), since the kinetic scheme and time constants are very similar in these two mutants. In addition, FTIR results on the same mutants show great

similarities, consistent with the present results (Zvyaga et al., 1996; Fahmy et al., 1994).

As in E113A/A117E, the batho decay of mutant G90D was faster than our time resolution (20 ns), which again argues for a faster chromophore relaxation than in rho. The "$C_{12}-C_{13}$" stretching mode (1238 cm^{-1} in rho) is shifted down to 1231 cm^{-1} (Fahmy et al., 1996), consistent with our previous hypothesis that this mode is sensitive to the same features that cause accelerated batho decay.

The G90D bsi and lumi intermediates show the same tendencies in λ_{max} values as those of E113A/A117E (Table 1), a pronounced blue shift for bsi and a small blue shift for lumi (with respect to the parent pigment). Therefore, we assume the same motion of the SB proton relative to its counterion as in E113A/A117E. This assumption is strengthened by the overall similarities of FTIR data on both mutants (Fahmy et al., 1994, 1996; Zvyaga et al., 1996) and the same kinetics up to lumi (Table 2). Remarkably, the red shift of G90D batho (+16 nm) was reduced relative to rho and the other mutants (31−36 nm) (Table 1). At −185 °C this red shift is even more reduced (Fahmy et al., 1996). The main difference in terms of location and orientation between G90D and the other mutants is that in G90D the counterion is attached to helix 2 and not helix 3. We assume that the reduced G90D batho red shift therefore originates from that difference.

As observed for E113A/A117E, a MI-like intermediate appears for mutant G90D. It was shown that this intermediate is the transducin-activating species by a combined FTIR and biochemical study (Zvyaga et al., 1996), as was the case for E113A/A117E. Therefore, once more we refer to this MI-like intermediate as R*. The most striking kinetic difference between G90D and E113A/A117E is the absence of a back-reaction from R* to lumi for G90D. This indicates that the thermal barrier of this particular back-reaction is substantially higher in G90D than in E113A/A117E. Changed energy barriers can be caused by different conformations of the intermediates, which should show up in the amide I bands of the FTIR measurements. In fact, the negative band at 1656 cm^{-1} and the difference band at 1695 cm^{-1} (negative)/ 1687 cm^{-1} (positive), which are one characteristic of the R* state, are reproduced in E113A/A117E but are almost absent in G90D (Fahmy et al., 1994; Zvyaga et al., 1996).

REFERENCES

Albeck, A., Friedman, N., Ottolenghi, M., Sheves, M., Einterz, C. M., Hug, S. J., Lewis, J. W., & Kliger, D. S. (1989) *Biophys. J. 55*, 233−241.

Arnaboldi, M., Motto, M. G., Tsujimoto, K., Balogh-Nair, V., & Nakanishi, K. (1979) *J. Am. Chem. Soc. 101*, 7082−7084.

Baldwin, J. M. (1993) *EMBO. J. 12*, 1693−1703.

Birge, R. R. (1990) *Biochim. Biophys. Acta 1016*, 293−327.

Birge, R. R., Einterz, C. M., Knapp, H. M., & Murray, L. P. (1988) *Biophys. J. 53*, 367−385.

Blatz, P. E., Mohler, J. H., & Navangul, H. V. (1972) *Biochemistry 11*, 848−855.

Einterz, C. M., Lewis, J. W., & Kliger, D. S. (1987) *Proc. Natl. Acad. Sci. U.S.A. 84*, 3699−3703.

Einterz, C. M., Hug, S. J., Lewis, J. W., & Kliger, D. S. (1990) *Biochemistry 29*, 1485−1491.

Eyring, G., Curry, B., Mathies, R. A., Fransen, R., Palings, I., & Lugtenburg, J. (1980) *Biochemistry 19*, 2410−2418.

Eyring, G., Curry, B., Broek, A., Lugtenburg, J., & Mathies, R. A. (1982) *Biochemistry 21*, 384-393.

Fahmy, K., Grossjean, M. F., Siebert, F., & Tavan, P. (1989) *J. Mol. Struct. 214*, 257−288.

Fahmy, K., & Sakmar, T. P. (1993) *Biochemistry 32*, 9165−9171.

Fahmy, K., Siebert, F., & Tavan, P. (1991) *Biophys. J. 60*, 989−1001.

Fahmy, K., Siebert, F., & Sakmar, T. P. (1994) *Biochemistry 33*, 13700−13705.

Fahmy, K., Siebert, F., & Sakmar, T. P. (1995) *Biophys. Chem. 56*, 171−181.

Fahmy, K., Zvyaga, T. A., Sakmar, T. P., & Siebert, F. (1996) *Biochemistry 35*, 15065−15073.

Franke, R. R., Sakmar, T. P., Graham, R. M., & Khorana, H. G. (1992) *J. Biol. Chem. 267*, 14767−14774.

Ganter, U. M., Gärtner, W., & Siebert, F. (1988a) *Biochemistry 27*, 7480−7499.

Ganter, U. M., Schmid, E. D., & Siebert, F. (1988b) *J. Photochem. Photobiol. 2*, 417−426.

Ganter, U. M., Schmid, E. D., Perez-Sala, D., Rando, R. R., & Siebert, F. (1989) *Biochemistry 28*, 5954−5962.

Ganter, U. M., Kashima, T., Sheves, M., & Siebert, F. (1991) *J. Am. Chem. Soc. 113*, 4087−4092.

Han, M., & Smith, S. O. (1995) *Biochemistry 34*, 1425−1432.

Han, M., DeDecker, B. S., & Smith, S. O. (1993) *Biophys. J. 65*, 899−906.

Han, M., Lin, S. W., Smith, S. O., & Sakmar, T. P. (1996) *J. Biol. Chem. 271*, 32330−32336.

Hofmann, K. P., Jäger, S., & Ernst, O. P. (1995) *Isr. J. Chem. 35*, 339−355.

Honig, B., Greenberg, A., Dinur, U., & Ebrey, T. G. (1976) *Biochemistry 15*, 4593−4599.

Honig, B., Dinur, U., Nakanishi, K., Balogh-Nair, V., Gawinowicz, M. A., Arnaboldi, M., & Motto, M. G. (1979) *J. Am. Chem. Soc. 101*, 7084−7086.

Hug, S. J., Lewis, J. W., Einterz, C. M., Thorgeirsson, T. E., & Kliger, D. S. (1990) *Biochemistry 29*, 1475−1485.

Imai, H., Mizukami, T., Imamoto, Y., & Shichida, Y. (1994) *Biochemistry 33*, 14351−14358.

Imamoto, Y., Sakai, M., Katsuta, Y., Wada, A., Ito, M., & Shichida, Y. (1996) *Biochemistry 35*, 6257−6262.

Jäger, F., Fahmy, K., Sakmar, T. P., & Siebert, F. (1994) *Biochemistry 33*, 10878−10882.

Kliger, D. S., & Lewis, J. W. (1995) *Isr. J. Chem. 35*, 289−307.

Kliger, D. S., Milder, S. J., & Dratz, E. A. (1977) *Photochem. Photobiol. 25*, 277−286.

Kojima, D., Imai, H., Okana, T., Fukada, Y., Crescitelli, F., Yoshizawa, T., & Shichida, Y. (1995) *Biochemistry 34*, 1096−1106.

Koutalos, Y., Ebrey, T. G., Tsuda, M., Odashima, K., Lien, T., Park, M. H., Shimizu, N., Derguini, F., Nakanishi, K., Gilson, H. R., & Honig, B. (1989) *Biochemistry 28*, 2732−2739.

Kuwata, D., Imamoto, Y., Okano, T., Kokame, K., Kojima, D., Matsumoto, H., Morodome, A., Fukada, Y., Shichida, Y., Yasuda, K., Shimura, Y., & Yoshizawa, T. (1990) *FEBS Lett. 272*, 128−132.

Lanyi, J. K., & Váró, G. (1995) *Isr. J. Chem. 35*, 365−385.

Lewis, J. W., & Kliger, D. S. (1993) *Rev. Sci. Instrum. 64*, 2828−2833.

Lewis, J. W., Warner, J., Einterz, C. M., & Kliger, D. S. (1987) *Rev. Sci. Instrum. 58*, 945−949.

Lewis, J. W., Einterz, C. M., Hug, S. J., & Kliger, D. S. (1989) *Biophys. J. 56*, 1101−1111.

Lewis, J. W., Liang, J., Ebrey, T. G., Sheves, M., & Kliger, D. S. (1995a) *Biochemistry 34*, 5817−5823.

Lewis, J. W., Pinkas, I., Sheves, M., Ottolenghi, M., & Kliger, D. S. (1995b) *J. Am. Chem. Soc. 117*, 918−923.

Lin, S. W., Sakmar, T. P., Franke, R. R., Khorana, H. G., & Mathies, R. A. (1992) *Biochemistry 31*, 5105−5111.

Lin, S. W., Imamoto, Y., Fukada, Y., Shichida, Y., Yoshizawa, T., & Mathies, R. A. (1994) *Biochemistry 33*, 2151−2160.

Mah, T. L., Lewis, J. W., Sheves, M., Ottolenghi, M., & Kliger, D. S. (1995) *Photochem. Photobiol. 62*, 356−360.

Nathans, J. (1990) *Biochemistry 29*, 9746−9752.

Palings, I., Pardoen, J. A., Van den Berg, E., Winkel, C., Lugtenburg, J., & Mathies, R. M. (1987) *Biochemistry 26*, 2544−2556.

Popp, A., Ujj, L., & Atkinson, G. H. (1995) *J. Phys. Chem. 99*, 10043−1045.

Rao, V. R., Cohen, G. B., & Oprian, D. D. (1994) *Nature 367*, 639−642.
Sakmar, T. P., & Fahmy, K. (1995) *Isr. J. Chem. 35*, 325−337.
Sakmar, T. P., Franke, R. R., & Khorana, H. G. (1989) *Proc. Natl. Acad. Sci. U.S.A. 86*, 8309−8313.
Schertler, G. F. X., & Hargrave, P. A. (1995) *Proc. Natl. Acad. Sci. U.S.A. 92*, 11578−11582.
Shichida, Y., Kropf, A., & Yoshizawa, T. (1981) *Biochemistry 20*, 1962−1968.
Shichida, Y., Okada, T., Kandori, H., Fukada, Y., & Yoshizawa, T. (1993) *Biochemistry 32*, 10831−10838.
Siebert, F. (1995) *Isr. J. Chem. 35*, 309−323.
Thorgeirsson, T. E., Lewis, J. W., Wallace-Williams, S. E., & Kliger, D. S. (1993) *Biochemistry 32*, 13861−13872.
Tokunaga, F., Iwasa, T., Miyagishi, M., & Kayada, S. (1990) *Biochem. Biophys. Res. Commun. 173*, 1212−1217.
Yan, M., Manor, D., Weng, G., Chao, H., Rothberg, L., Jeddju, R. R., & Callender, R. H. (1991) *Proc. Natl. Acad. Sci. U.S.A. 88*, 9809−9812.
Zhukovsky, E. A., & Oprian, D. D. (1989) *Science 246*, 928−930.
Zvyaga, T. A., Min, K. C., Beck, M., & Sakmar, T. P. (1993) *J. Biol. Chem. 268*, 4661−4667.
Zvyaga, T. A., Fahmy, K., & Sakmar, T. P. (1994) *Biochemistry 33*, 9753−9761.
Zvyaga, T. A., Fahmy, K., Siebert, F., & Sakmar, T. P. (1996) *Biochemistry 35*, 7536−7545.

BI962320U